Effects of crumb rubber size and percentage on degradation reduction of railway ballast

Guo, Yunlong; Markine, Valeri; Qiang, Weile; Zhang, Hui; Jing, Guoqing

DOI
10.1016/j.conbuildmat.2019.03.315

Publication date
2019

Document Version
Accepted author manuscript

Published in
Construction and Building Materials

Citation (APA)
Guo, Y., Markine, V., Qiang, W., Zhang, H., & Jing, G. (2019). Effects of crumb rubber size and percentage on degradation reduction of railway ballast. *Construction and Building Materials*, *212*, 210-224. https://doi.org/10.1016/j.conbuildmat.2019.03.315

Effects of crumb rubber size and percentage on degradation reduction of railway ballast

Yunlong Guo [1], Valeri Markine [1], Weile Qiang [2], Hui Zhang [3], Guoqing Jing [2 *]

1. Faculty of Civil Engineering and Geosciences, Delft University of Technology, Delft, 2628CN, Netherlands

2. School of Civil Engineering, Beijing Jiaotong University, Beijing, 100044, China

3. Ruihai 3D technology limited company, Beijing, 100029, China

*. Corresponding author

Email addresses: yunlong.guo@tudelft.nl (Y. Guo); gqjing@bjtu.edu.cn (G. Jing)

Abstract

Higher speed, more freight and frequent maintenance increase ballast degradation and reduce the ballast lifespan. To reduce ballast degradation, crumb rubber used as buffering aggregates in ballast bed is relatively unexplored and needs more studies, because using it has the advantage of reusing the waster rubber and absorbing the noises. The effects of crumb rubber (CR) size and percentage on ballast degradation reduction is studied in this paper, and the optimal CR size and percentage are proposed. Three CR size ranges are utilised, i.e., 3~5 mm, 10~15 mm and 20~25 mm, and the percentages are 0, 10, 20 and 30% by weight. Three kinds of ballast material with two size ranges are utilised. The deteriorated ballast particles were generated using Los Angeles Abrasion (LAA) tests, and the ballast degradation was evaluated with the 3D image analysis. The results indicate that ballast abrasion can be alleviated by adding the CR, while the CR has few influences on the ballast breakage. When CR size is close to ballast particle size, the effects of degradation reduction are not obvious. The corner and edge loss are the main types of ballast abrasion, although different ballast materials significantly influence the abrasion type and degree. Most importantly, the image analysis method is proved to have the ability to present ballast degradation process and has great potential for further degradation-related studies.

Key words: Los Angeles Abrasion test; Three-dimensional image analysis; Ballast degradation; Crumb rubber

1 Introduction

Ballast track plays a significant role in the transportation infrastructure, and it is widely used worldwide. As the main part of ballast track, the ballast bed helps to transmit and distribute wheel loadings and vibrations from sleepers to the subgrade, providing water drainage, sufficient lateral and longitudinal resistance, suitable resiliency and energy dissipation [1]. Although it is required in all the standards from different countries that the materials for ballast should be hard, durable, and unweathered, the ballast bed still deteriorates due to ballast breakage and abrasion/wear, inducing the unacceptable track deformation, frequent tamping and finally ballast renewal [2].

To prolong the ballast service life, researchers have developed ample practical application of new materials in ballast track in recent decades, such as under sleeper pads (USP), geogrid, and polyurethane. Among them, the most favourite method is the USP. It reduces the ballast degradation

by softening the sleeper-ballast interface, increasing the contact areas and the number of load-bearing sleepers, and then diminishing the pressures to ballast [3-5]. Another method, the geogrid is also widely used in the fresh and foul ballast to increase the shear strength and apparent angle of shearing resistance [6], and it can restrict lateral displacement of ballast, reduce settlement as well as minimise ballast degradation [7]. Bonding the ballast particles with polyurethane is popular due to the effects of improving the strength and resiliency of the ballast bed and reducing permanent track settlement, especially in some special areas (e.g. transition zones) [8, 9]. However, high costs are the main limitation to the USP and the polyurethane, while the geogrid application is limited by the construction and maintenance tasks, e.g. the tamping operation.

Towards these limitations, the reuse of waste rubber in ballast bed is proposed as a solution, but few studies on this have been performed. This topic is necessary and worthwhile to study because it can reduce the ballast degradation [10, 11], absorb noises [12-14] and dispose waste rubber (low costs). However, due to the limited numbers of research, the studies did not always reach the same conclusion. For instance, reducing the ballast degradation was proved in [10, 11], nevertheless, the two studies reported different results on the optimal percentage of the CR. Both of them proposed 10% is the optimal percentage. Interestingly, the percentage is by volume in [10], whereas in [11] the percentage is by weight.

Besides the optimal percentage, another research gap is the effects of the CR size on the ballast degradation reduction. Some of earlier studies utilised the same Particle Size Distribution (PSD) as the ballast [11, 15], while most of the other studies utilised smaller rubber sizes under 20 mm [10, 12, 16]. Even though the studies proved the addition of the CR can reduce ballast degradation and absorb the vibration, the results can be more reliable and useful when the rubber size is confirmed. Because the studies of sand-rubber mixture behaviour in [17] showed clear size effects of the CR on the mechanical behaviour of the mixture. In addition, the mixture can influence the degradation process. However, research on the degradation reduction of ballast-rubber mixture (size effects) is still relatively unexplored until now.

In response to these research gaps, this paper aims to study the effects of mixing the CR with ballast particles on the ballast degradation reduction. To achieve the aim, a set of LAA tests were performed on three kinds of ballast (materials) mixed with a different amount of the CR (i.e., 0, 10, 20 and 30% by weight). Additionally, the CR sizes used in this study are 3~5 mm, 10~15 mm and 20~25 mm. The LAA test was utilised to produce impacts to the ballast for accelerating ballast degradation artificially, and then the ballast degradation is evaluated by analysing the 3D particle images. The image analysis is applied in this study, because earlier methods (based on sieving) may not sufficiently quantify the ballast degradation.

Therefore, this paper focuses on using image analysis method to quantify the ballast degradation (three kinds of material) mixed with various percentage and size of the CR, with the LAA test to provide artificial impact to the mixes. The high-precision laser scanner is used to obtain the three-dimensional (3D) images of ballast particles at different drum turns. Based on the images, the change of the initial and final morphology can be calculated. Subsequently, the ballast degradation can be quantified. These results can indicate using the CR is an effective method to attentive ballast degradation, providing a lead application of waste rubber for railway engineering.

2 Materials and methods

2.1 Material properties

As shown in Figure 1, the ballast materials used in the present tests are from three primary rocks (i.e. granite, sandstone, volcanic) from Qian'an, Tai'an and Lulong, respectively. The material can be described as uniformly graded, hard gravel. Their physical properties are estimated with the Chinese

standard and British standard [18, 19], which concludes that the materials are suitable utilised as railway ballast. The basic characterisations of the ballast materials are given in Table A.1. The CR used for the test is a scrap railway product (i.e. rail pad), free of steel wires provided by Zhejiang Tiantie Industry. Its elastic modulus is 8 MPa. All the ballast and rubber particles were washed, dried, and cooled at room temperature before testing.

The ballast and rubber particles were sieved and selected to obtain the desired size ranges for the tests. The samples subjected to the LAA tests were the mixtures of ballast and CR particles. Two size ranges of ballast particles are 30~35 mm and 40~45 mm, mixed with one size range of the CR. Three size ranges of the CR were used, which are 3~5 mm, 10~15 mm and 20~25 mm. The CR percentages are 0, 10, 20, 30%.

The CR size and shape selection criterion is according to the following aspects: (1) the CR size should be smaller than the ballast particles due to larger CR has less influences. In other words, when the rubber particle size exceeds 25 mm, the effects on ballast degradation reduction is not obvious. More importantly, when the CR size is too big, the ballast interactions are weakened by reducing ballast interactions, which leads to more settlement in the real track. (2) Two CR particle forms (irregular and cuboid) are respectively mixed with ballast particles, and the LAA tests were performed on them. Their LAA loss results are approximately the same, thus, the easily obtained form (cuboid) is chosen in this study. (3) The CR percentage selection is according to the references [10, 11], furthermore, it is also considered that when the percentage is over 30%, all the ballast voids are jammed. Consequently, the maximum percentage is selected at 30%. Afterwards, reducing the percentage by 10% can have the three recognizable result differences. Particularly, when the percentage differences are too small, the result differences are extremely hard to distinguish due to the irregular characteristics (morphology, inside crack) of ballast particles.

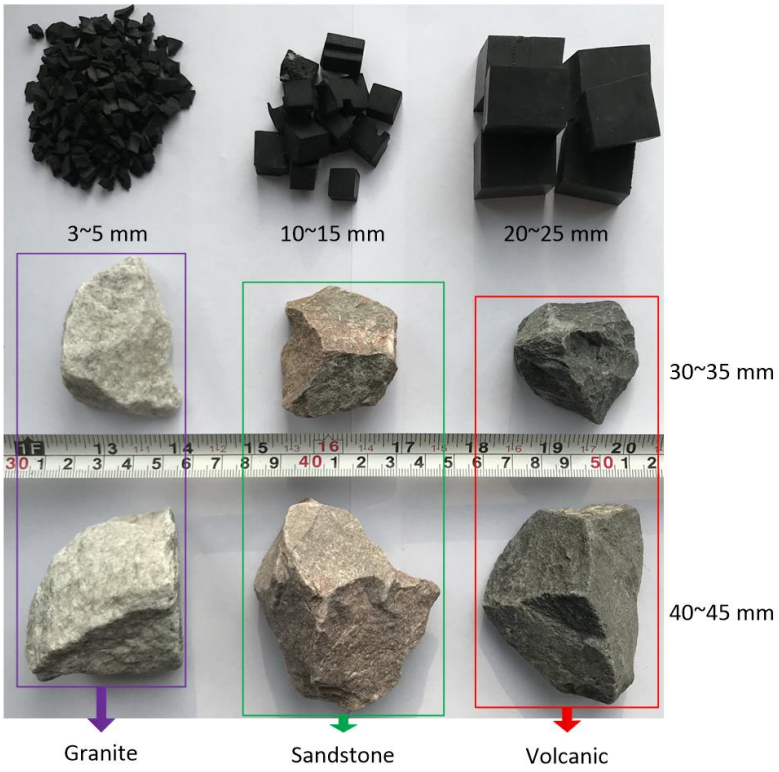

Figure 1 Ballast and crumb rubber particles

2.2 Method description

The LAA tests are combined with the laser scanning to compare the effects of various CR sizes and percentages on the degradation reduction of ballast particles. The test flow chart is shown in Figure 2.

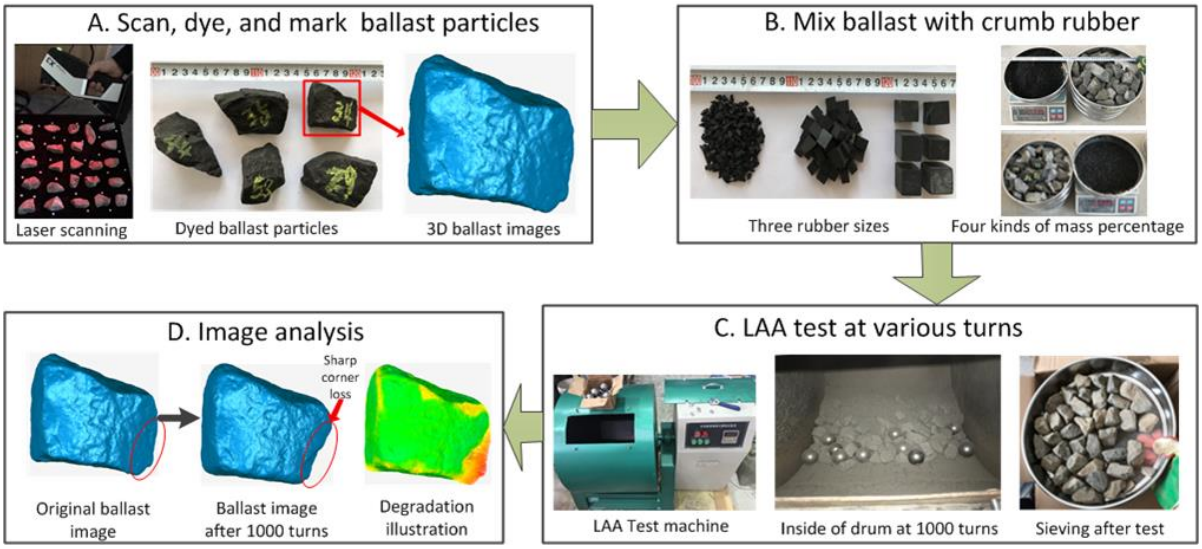

Figure 2 Test flow chart (the image of laser scanning is reproduced from [20])

The first step includes scanning, dyeing and marking the ballast particles. With laser scanning, the initial geometries of the ballast particles are recorded by their 3D images. Dyeing is coating the ballast particles in ink and this means has been successfully applied in plenty of studies, e.g. [21, 22]. Marking is to number the ballast particles. Afterwards, five scanned/dyed/marked ballast particles together with the other ballast particles are homogeneously mixed with the CR at the designated percentage. The LAA tests are performed on the CR-ballast mixtures with various drum turns (i.e. 1000, 2000). After that, the samples are sieved and weighed, and the five scanned/dyed/marked ballast particles in each sample are sought out and performed the second time laser scanning. Finally, the image analysis is implemented with the 3D images.

2.2.1 Laser scanning

The FreeScan X5 laser scanner is a portable handheld 3D laser scanner, and its parameters are given in Table 1. It has been optimised to satisfy the need of flexible and convenient scanning ballast particles at high accuracy and stability. The reason for choosing this laser scanner is that it is efficient to obtain 3D ballast images by scanning many particles at the same time (Figure 2A). The single shot accuracy describes the error of one shot is within a value. The volume precision presents the cumulative error when measuring large objects. The resolution describes the shortest distance between two scanned points that can be captured. The scan depth is the largest vertical distance that can be captured by the scanner.

Table 1 FreeScan X5 laser scanner properties

Property	FreeScan X5
Weight	0.95 kg
Dimensions (L × W × H)	130 × 90 × 310 mm
Single shot accuracy	0.035 mm
Volume precision	0.02 mm + 0.08 mm/m
Resolution	0.1 mm
Scan speed	350,000 scan/s
Scan range	100~8000 mm
Working distance	300 mm
Scan depth	250 mm
Light source	10-line laser ray

The scanning operation was performed on some certain ballast particles before LAA tests. Limited numbers of ballast particles were scanned instead of the whole sample because the scanning operation and 3D image processing cost large amounts of time. Towards this issue, five typical ballast particles for one sample (49 samples in total) were selected for scanning, and the five selected particles are almost the same size but with different shapes (i.e. four cubic and one non-cubic), as shown in Figure 3A.

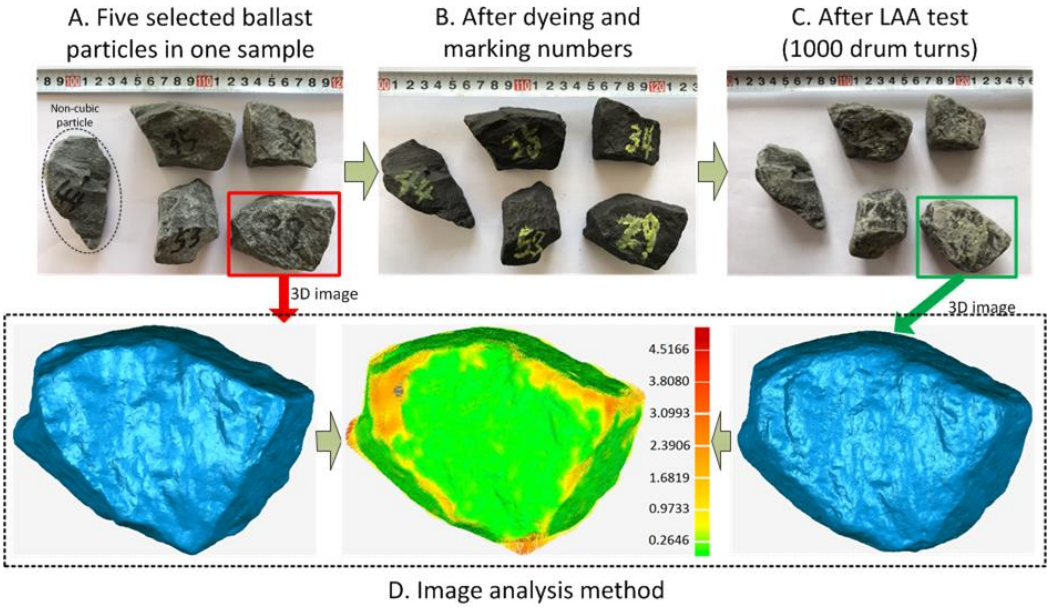

Figure 3 Five selected ballast particles in one sample and the image analysis method

The scanned ballast particles were marked and dyed (Figure 3B), in order to distinguish them after 1000 drum turns. After seeking them out, they were washed, dried and scanned again (Figure 3C). The same procedure was performed again on the scanned ballast particles, including the dyeing, marking, LAA test (1000 drum turns) and laser scanning. That is for analysing the ballast degradation degree at different degradation stages. The 3D images of one particle were compared to quantify the degradation using the image analysis method, which will be introduced in the Section Image analysis method.

2.2.2 LAA test

The LAA test is utilised in this study to generate artificial impacts on the ballast particles. The LAA test is a classic method to measure resistance to toughness reduction or a breakage tendency of coarse aggregate and the most widely used for aggregate qualification throughout the world. In the LAA test, the mixture together with 12 steel balls is put into the LAA test drum. The rubber and ballast are homogeneously mixed before putting into the drum. In Figure 2C, it shows 12 steel balls and drum used for LAA test, and the drum is with the inside diameter at 71 cm and rotates around the horizontal axis (30~33 rpm). The test configuration and machine meet the requirement of the British Standard and Chinese standard [18, 19].

Regarding the methods to generate deteriorated ballast, several laboratory tests can be utilised, such as micro-Deval abrasion test, ballast box test, as well as LAA test [23]. The LAA test is chosen in this study because it can rapidly deteriorate ballast particles and have advantages over the other two. In the LAA test, the ballast particles deteriorate rapidly, due to not only the attrition between rock particles but also the impacts from steel balls [24]. As concluded in [24], the LAA test is better than micro-Deval abrasion test to simulate the real material breakdown. Moreover, when tamping is considered in ballast box tests, the LAA test results correlate well with the ballast box results [25-27].

Using the LAA machine for generating ballast degradation in this study has other reasons as well.

- It is easier to control the degradation degree (by drum turns) in the laboratory tests than the in-site tests. Additionally, the LAA test is easier to crush ballast particles than other experimental tests, e.g., the micro-Deval test.
- A steel shelf in the drum and towards the axis is used for lifting and dropping the ballast sample and steel balls, which produces the impacts.
- With the drum rotating, the wear and abrasion can be treated as the loading.
- It is much faster to obtain the deteriorated ballast particles than from the operating line, which mostly needs years.

The LAA test was performed after laser scanning the certain ballast particles, and two times were performed on the same sample with the drum turns of each time at 1000. After every 1000 turns, the LAA loss is calculated with Equation 1. In the equation, M_1 is the initial weight of tested ballast particles, and the M_2 is the weight of the tested ballast particles after the LAA test, which cannot pass the 1.6 mm sieve. It needs to note that a sample was performed the LAA test without steel balls to check the effects of steel balls on the ballast degradation. Because the impacts from steel balls may dominate the degradation by crushing the ballast particles.

Equation 1 $$LA = 100 \times (M_1 - M_2) / M_1$$

Traditionally, the LAA test uses results from sieving for material quality evaluation or degradation evaluation. The material quality is evaluated with the LAA loss (Equation 1), which is the mass percentage that passes the 1.6 mm sieve compared to the original mass. The LAA loss can present the size reduction due to impacts and attrition as concluded in [28]. Regarding the degradation evaluation, almost all the methods are based on the particle size distribution (PSD). The PSD is a curve presenting the mass percentage that could pass some certain sieve sizes.

However, it may not be accurate to evaluate the ballast degradation with the sieving methods, because sieving does not essentially measure the size of any of the particles in the sample [28]. It only presents the smallest particle projection that can pass the sieve mesh. The results are influenced by particle shape and rely on the sieving duration in most cases [29]. Therefore, sieving is not an accurate method for measuring how much the particles reduce in size or shape due to the LAA test. In other words, it is not sufficient to evaluate ballast degradation.

2.2.3 Image analysis method

Ballast degradation has two types, abrasion and breakage. The method proposed in [30] is used for abrasion analysis in this study, while the breakage is evaluated with a modified 3D image analysis method.

Because of higher accuracy, the image analysis method was chosen in this study to evaluate ballast degradation, and the ability to evaluate degradation has been verified in plenty of studies [23, 30, 31]. Ballast degradation is evaluated by quantifying the changes of the particle morphology. The particle morphology is quantified with the particle geometrical properties (e.g. volume, surface area, three axial lengths), and the geometrical properties are calculated by analysing the particle images.

Initially, 2D images are used for particle morphology evaluation [32, 33], and with the technical tools developing, the 3D image can be obtained and analysed for more accurate morphology evaluation [34]. With the particle morphology evaluation, ballast degradation can be quantified by comparing the morphology and calculating the morphology changes during degradation. For example, the change of a morphological index (Flat and elongated ratio) was used for degradation evaluation in [23]. The index is calculated with the three axial lengths of the particle, and the lengths are obtained

by analysing one particle's three images, which are taken with three cameras at orthogonal views, as shown in Figure 4.

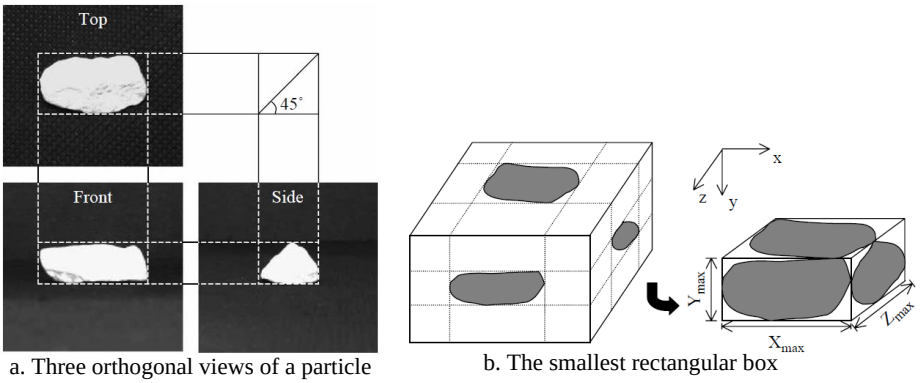

a. Three orthogonal views of a particle b. The smallest rectangular box

Figure 4 Each view of the 3 cameras for one particle (front, top, and side) and the box (framework) for dimension determination (figure reproduced from [35])

However, there exist limitations when using the earlier image analysis methods. One limitation is using 2D images is not accurate for morphology evaluation. For example, the particle volume (a morphological index) is calculated with errors. As reported in [36], the average absolute error is at 11.5%. To reduce the error, it needs to use large amounts of 2D images for one particle [37], which is quite time-consuming. Most importantly, the volume loss is utilised as an important index to quantify ballast degradation in this study [30].

Another limitation is that the types of ballast breakage cannot be confirmed. It is significant to confirm that because the breakage types have great influences on the change of the PSD, and further influence the performance of ballast bed. The PSD change or checking the particles under some certain size were utilised in most studies to quantify ballast breakage. Even though with the image analysis the PSD can be measured more accurately, the breakage types can still not be confirmed.

Towards these limitations, 3D images are analysed to evaluate ballast abrasion in this study, and a modified 3D image analysis method is utilised for ballast breakage. Analysing 3D images is accurate to calculate the particle volume. As reported in [38], the error can be within 0.1%. The image analysis method used in [30] can identify the ballast breakage, calculating the number percentage of broken ballast particles. The new method is to modify it to obtain ballast breakage types.

Specifically, as shown in Figure 5, an example of a ballast breakage type is illustrated. After the LAA test, the scanned ballast particles are easy to find out, and they are compared with their initial images to match, according to the remained colour and marked numbers. Afterwards, the ballast breakage type can be easily confirmed, and the ballast abrasion can be analysed with the Abrasion Depth [30].

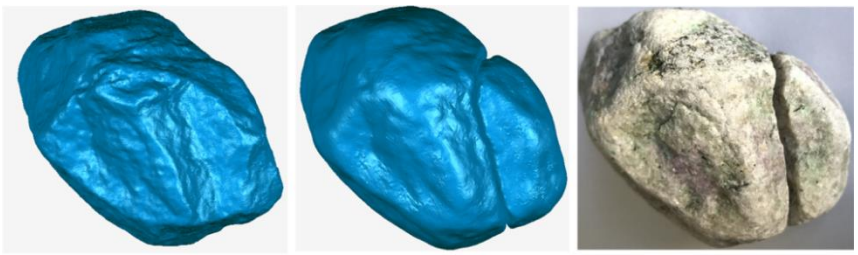

A. Particle image before LAA test | B. Particle image after LAA test | C. Ballast Particle after LAA test

Figure 5 Example of ballast breakage type

The Abrasion Depth is the image analysis method (Figure 3D) that calculates the distances of two images after alignment. In the figure, it can be observed the values (unit, mm) on the right side are corresponding to the distances according to colours. Two types of Abrasion Depth were proposed, the Maximum Abrasion Depth (MAD) and the Average Abrasion Depth (AAD). The MAD is the largest distance between the two images, and the AAD is the average of all the distances. More explanations can be found in [30].

The new method for ballast breakage quantification is based on the total surface area change. After a ballast particle crushes into two or more pieces, its total surface area increases. The ratio of the total surface area change to the product of intermediate and shortest dimensions is defined as the breakage index (*BI*), as shown in Equation 2. In the equation, A_1 is the total surface area after breakage, and A_2 is the surface area before breakage; *b* is the intermediate dimension of the particle, and *c* is the shortest dimension (Figure 4).

Equation 2 $$BI = (A_1 - A_2) / (b \cdot c)$$

3 Results and discussion

3.1 LAA loss results

3.1.1 Crumb rubber size and percentage

The LAA loss results of different CR size ranges (i.e. 3~5/10~15/20~25 mm) and percentages (i.e. 0/10/20/30%) are given in Appendix A (Table A.2). Based on the table, the results are compared and illustrated in Figure 6. The ballast material is volcanic and the size is 40~45 mm in Figure 6 A~F.

From Figure 6 A/B/C, it can be observed that the LAA loss decreases with the increasing CR percentage. For the CR size at 3~5 mm, the LAA loss of the percentage 10% is almost the same as 20%, while 30% has the lowest LAA loss. For the CR size at 10~15 and 20~25 mm, increasing CR percentage over 10% (i.e. 20%, 30%) does not have a significant effect on the LAA loss reduction, especially the drum turns from 1000 to 2000.

In Figure 6 D/E/F, the CR size at 3~5 mm has the lowest LAA loss, while the 20~25 mm has the highest value. This discipline can also be observed in Figure 6G, and this figure also demonstrates the LAA loss after the second 1000 drum turns is lower than that of the first 1000 turns. It needs to note that from the results of different drum turns, the degradation of different stages (i.e. first and second 1000 drum turns) can be seen. When it comes to Figure 6 H&I, the degradation at the two stages of some lines shows a different trend, which is that the second stage has higher LAA loss than the first. That is for the reason that the ballast material illustrated in the two figures (granite) is easier to crush than the volcanic. The breaking conditions of the two materials were observed during the LAA tests.

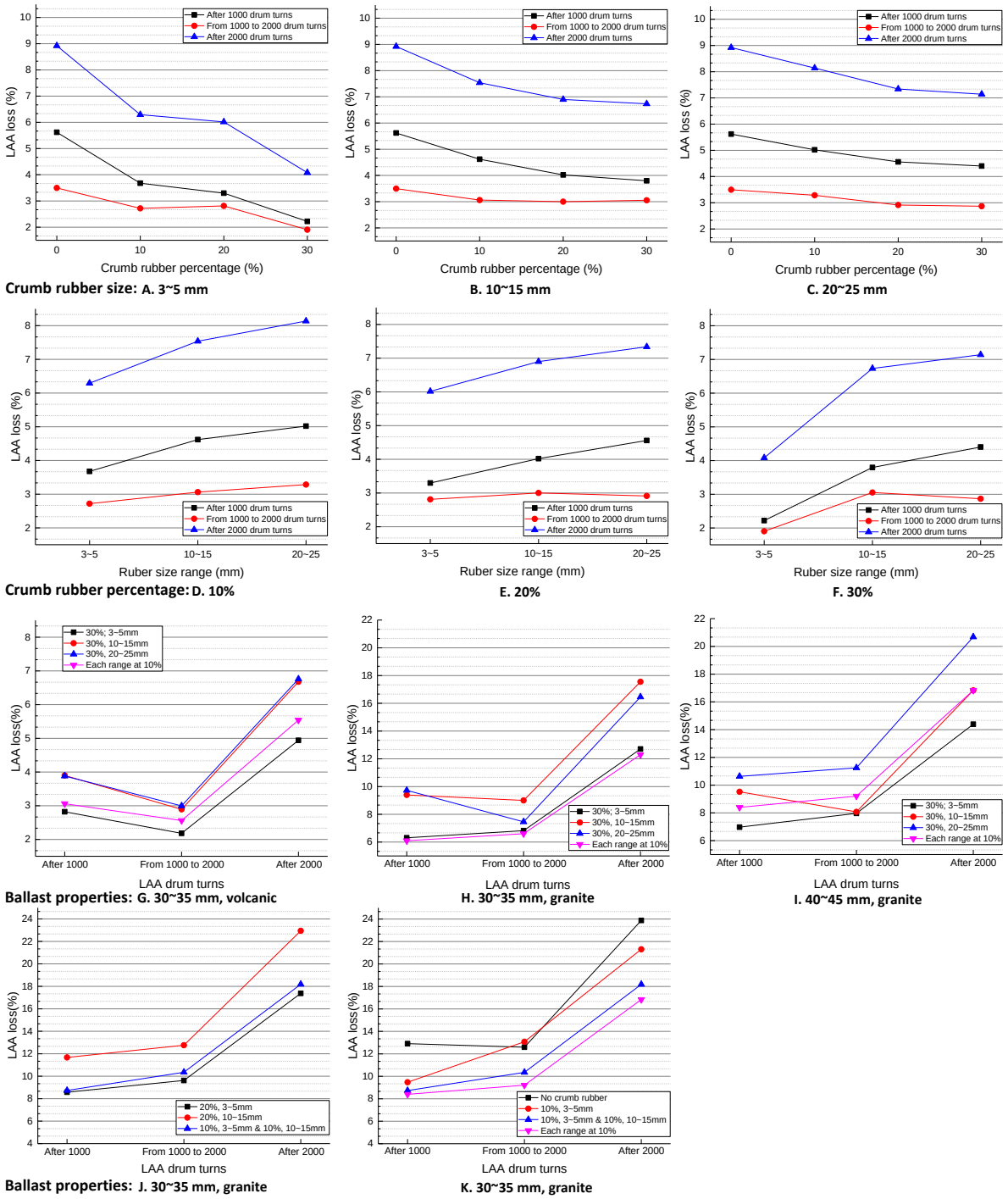

Figure 6 Los Angeles Abrasion test results concerning crumb rubber size and percentage

According to Figure 6 G/H/I, it can be seen that either each range at 10% or the 30% 3~5 mm CR has the lowest LAA loss. The each rang at 10% is the mixture of 10% 3~5 mm, 10% 10~15 mm and 10% 20~25 mm CR. Also, after comparing Figure 6G with Figure 6H, it can be observed that for the difficult breakage material (volcanic), the 3~5 mm CR is better at reducing the LAA loss, while for the granite (easily broken), the mixture of CR has a slightly better performance. However, when the ballast particles are at the size range of 40~45, the 30% 3~5 mm CR has lower LAA loss than the other three (Figure 6I). That means the CR size should be different for different ballast materials and sizes.

Figure 6 J&K illustrate how the mixtures of different CR sizes influence the ballast degradation. In Figure 6J, the mixture of 10% 3~5% mm and 10% 10~15 mm CR has approximately the same LAA loss

with the 20% 3~5 mm, but much lower than the 20% 10~15 mm after first 1000 drum turns. This discipline can also be observed in Figure 6K, specifically, the 10% 3~5 mm, the mixture (10% 3~5 mm and 10% 10~15 mm) and the mixture of each range at 10% have almost the same LAA loss after first 1000 drum turns. However, after the second 1000 drum turns, the two mixtures reduce the LAA loss much more than the 10% 3~5 mm. Moreover, the mixture of 10% 3~5 mm and 10% 10~15 mm has slightly higher LAA loss than that of each range at 10%. That is due to at the first 1000 drum turns, the 10% 3~5 mm plays the significant role of reducing the LAA loss while adding the other two size ranges (10~15, 20~25 mm) can reduce the value dramatically during the second 1000 drum turns, especially the 10% 10~15 mm.

From the results, the CR size and percentage should be different for various situations. Although adding more CR can reduce more LAA loss, however, when the percentage is over 10%, the LAA loss reduction is not obvious. Moreover, the CR size at 3~5 mm reduces the LAA loss most compared with the other two (i.e. 10~15, 20~25 mm). However, sometimes the CR mixture with different sizes has better performance for some certain ballast particle sizes and materials. Therefore, the following section is focusing on the ballast materials and sizes.

3.1.2 Ballast material and size, steel balls

Three kinds of ballast material were used in this study, and each of them has two particle size ranges (i.e. 30~35, 40~45 mm). As shown in Figure 7 A/B/C, the effects of the CR on different ballast sizes are different (after 2000 drum turns). From the figures, it can be observed that the large size ballast particles have a lower LAA loss. Additionally, with the CR percentage increasing, the LAA loss reduction of 30~35 mm is more obvious than that of 40~45 mm.

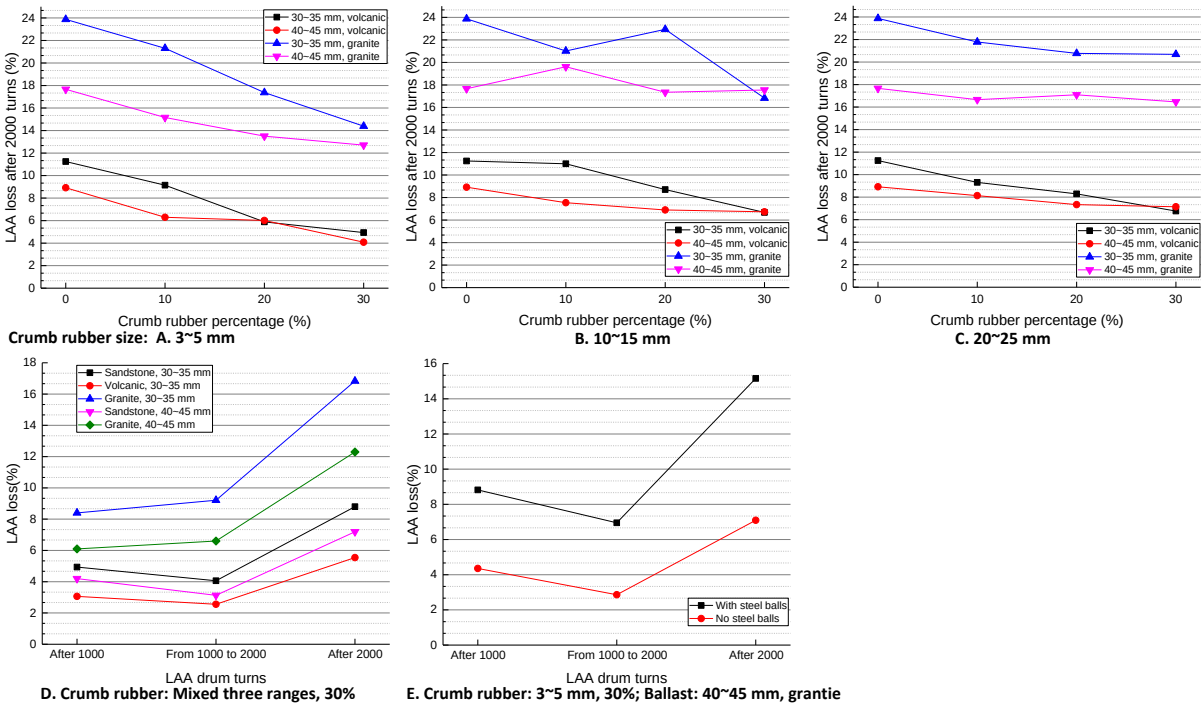

Figure 7 Los Angeles Abrasion test results concerning ballast size, material and steel balls

In Figure 7D, it can be observed that the sandstone and volcanic LAA loss of the first 1000 drum turns is higher than that of the second 1000 drum turns, while the granite is opposite. The mixed CR is each range at 10%, 30% in total. However, in Figure 7E, this trend cannot be observed. That is due to the CR size has great influences on the ballast degradation, the 30% 3~5 mm CR has better performance than the other two sizes.

In most of the LAA tests, the granite was easy to crush during the LAA tests, while the other two were not. Because most of the ballast particles lost the easily-lost parts (weak points, e.g. sharp corner, edge) during the tests [30], and breakage will produce new sharp corners and edges. Most importantly, different breakage types have significant influences on the numbers of weak points. Because of that, the particle breakage type will be analysed in details in Section 3.2.4, Breakage analysis.

The steel balls were considered in this study as a variable. Due to the steel balls, the LAA test is more prone to crush particles than the other tests (e.g. micro-Deval test). From Figure 7E, it can be observed that without steel balls, the LAA loss is much lower. The LAA test is more prone to abrade and crush ballast and the contribution from the steel balls is quite nonnegligible. For example, the steel balls are utilised in the micro-Deval test as well, but it rarely crushes ballast particles. More importantly, during the drum rotates, the broken particles have more sharp corners and edges, which are easy to lose weight (abrasion). In addition, ballast breakage produces more pieces of ballast particles, which provide more contacts not only between the ballast particles themselves but also between the drum/steel balls and the ballast particles.

According to the above results, some phenomena are easy to explain and as expected, while some are anomalous. In most cases, that is due to the ballast particles in each sample are different, e.g., the morphology (size and shape). The two variables are extremely hard to control, and according to [30], they have great effects on the results. Consequently, the individual ballast particles are analysed using the image analysis method.

3.2 Image analysis results

3.2.1 Volume and surface area

The volume and surface area of the scanned ballast particles can be obtained with 3D image analysis (given in Table A.3), as proposed in [34]. Based on the volume and surface area results, the volume loss and surface area loss can be calculated and given in Table A.4 (Appendix A). The volume loss is calculated by the ratio of the volume difference to the initial volume, while the surface area loss is the ratio of the surface area difference to the initial surface area. The average volume loss and average surface area loss are respectively calculated by averaging all the values in each group. It needs to note that the broken ballast particles and large corner loss particles were not included in the calculation.

From Table A.4, it can be seen that the volume and surface area of every individual particle reduce after LAA tests. That is as expected because the broken particles were not included. When a particle crushes into two or more pieces, the surface area will increase. This will be discussed later in Section 3.2.4, Breakage analysis.

According to Table A.4, it can also be observed that the average volume loss is mostly lower than the LAA loss at the rate of 43/49 (after 2000 drum turns). That means 6 groups of 49 groups are higher, and 5 groups of the 6 groups are the material, volcanic. Because the broken ballast particles were not included in the calculation, it is easy to understand that the average volume loss is lower. The higher average volume loss results from the scanned particles crushed and lost small parts after LAA tests, and these parts were not found or picked out for laser scanning. As shown in Figure 2D, it can be seen that one sharp corner of the particle is completely lost.

However, in the results of the second 1000 turns, only one group has higher average volume loss than the LAA loss. That means the easily-lost parts have already been lost (hypothesized in the last section). This can also be proved by that the average volume loss after the second 1000 drum turns is lower than the first 1000 turns, as shown in Table 2.

Table 2 Average volume loss of 49 groups

Group	1	2	3	4	5	6	7	8	9	10	11	12	13
First 1000 turns (%)	2.99	3.56	2.87	6.61	3.71	2.91	3.02	3.61	2.85	3.37	5.57	5.74	8.07
Second 1000 turns (%)	1.55	2.4	2.09	1.59	2.24	2.48	2.08	1.92	2.67	2.36	2.07	1.95	3.36
Group	14	15	16	17	18	19	20	21	22	23	24	25	26
First 1000 turns (%)	3.32	6.56	4.69	2.83	4.18	2.6	2.5	4.91	13.51	8.41	5.99	5.2	8.93
Second 1000 turns (%)	2.04	3.03	1.93	1.28	2.73	2.53	1.66	1.63	6.17	3.02	3.43	2.95	7.11
Group	27	28	29	30	31	32	33	34	35	36	37	38	39
First 1000 turns (%)	8.63	6.28	7.22	9.41	11.03	6.64	7.73	5.94	9.66	5.39	6.85	9.86	5.35
Second 1000 turns (%)	4.44	4.34	3.28	4.19	3.59	5	3.44	3.49	3.39	2.73	5.24	4.04	4.41
Group	40	41	42	43	44	45	46	47	48	49			
First 1000 turns (%)	8.34	5.11	6.58	5.72	5.71	5.46	3.51	4.86	5.78	4.26			
Second 1000 turns (%)	2.91	3.18	3.83	3.72	3.81	2.11	2.19	3.03	1.42	2.46			

The average volume loss and average surface area loss are compared with the LAA loss, as shown in Figure 8. From the figure, it can be seen that the average volume loss curve fits well with the average surface area loss curve, but mostly, they do not have the same trend with the LAA loss curve, such as Figure 8 C/E/F.

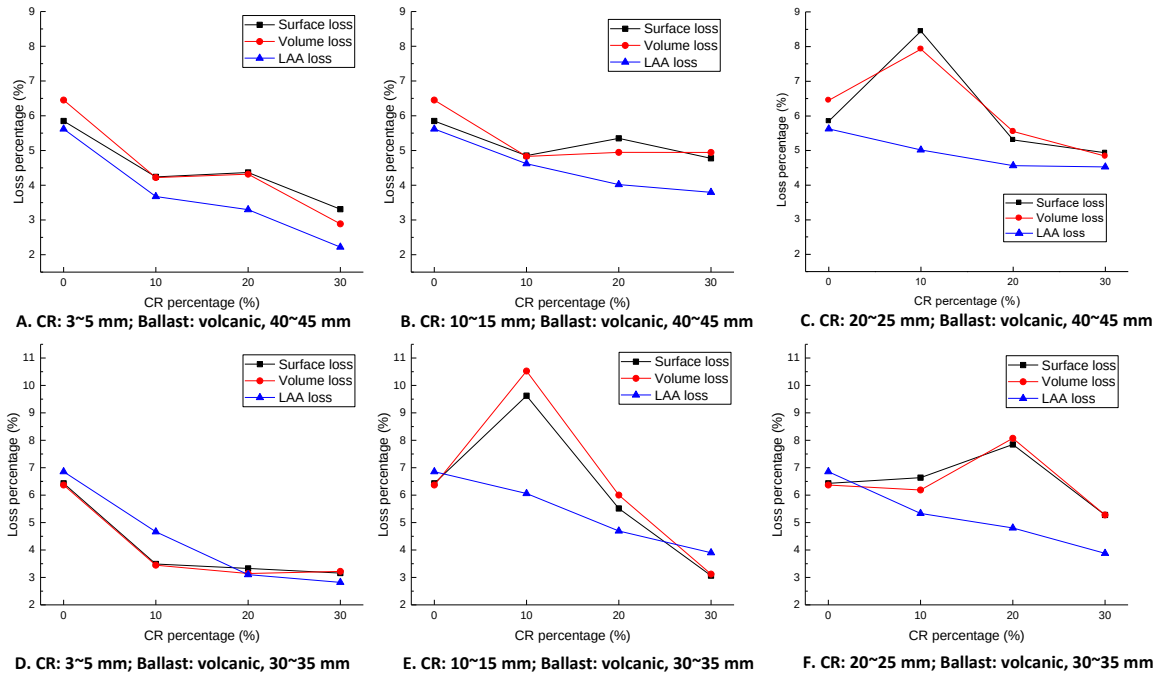

Figure 8 Comparison of average volume loss, average surface area loss and LAA loss (ballast material, volcanic)

This discipline is also discovered in the tests that used other ballast materials (i.e. granite), as shown in Figure 9. Moreover, in this figure, a larger difference value between average volume loss (or average surface area loss) and LAA loss can be observed. That is due to the granite is easier to crush than the volcanic, and the small fragment cannot be found or picked out for laser scanning.

According to the result in Figure 8 and Figure 9, it was found that only using the average volume loss or average surface loss for degradation evaluation is difficult to draw the conclusion. For example, in

Figure 8C, adding 10% 20~25 mm CR has a higher value than the group without CR. Also, in this figure, it can be seen that the LAA loss at 30% is higher than the other three LAA loss values.

An important reason for this phenomenon is that the morphology (size and shape) of ballast particles in every group cannot keep the exact same. Therefore, using the whole sample mass loss (i.e. LAA loss) or the average volume/surface area loss for degradation evaluation is not accurate. Towards this issue, the morphology of the scanned ballast particles are quantified first, and then the particles with similar quantified values are compared to check the effects of CR on the ballast degradation reduction.

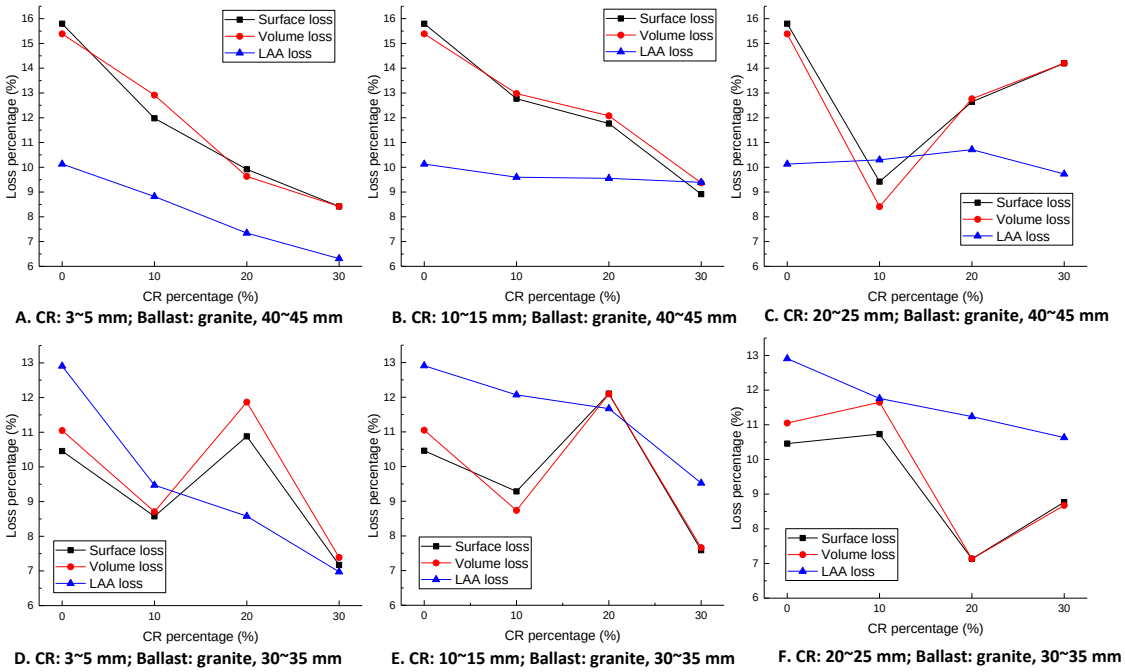

Figure 9 Comparison of average volume loss, average surface area loss and LAA loss (ballast material, granite)

3.2.2 Particle morphology evaluation

The particle morphology was quantified with morphological indices using 3D image analysis methods. For the particle shape, it is described with three characteristics, including the form, the angularity and the surface texture, which is the most widely-accepted description. Because each of them is independent and can be different without influencing the other two characteristics [39]. For the particle size, the volume, surface area or three particle dimensions can be utilised to quantify it. The three dimensions can be defined as the particle lengths at three views, as shown in Figure 4. The morphological indices for shape (three characteristics) and size are given below (Table 3).

In Table 3, the morphological indices for shape are calculated based on the volume, surface area and the three dimensions, which can be measured with the 3D image analysis method proposed in [34]. The calculation methods for the 3D True Sphericity and the Roundness are given in the reference [30, 40], respectively.

Table 3 The morphological indices for size and shape

Shape	Characteristics	Morphological index	Value range	Size	Morphological index	Value range
	Form	3D True Sphericity	0.75-0.85		Volume (mm^3)	35000-40000 (ballast size: 40~45 mm) 20000-32000 (ballast size: 30~35 mm)
	Angularity	Roundness	0.10-0.13		Surface area (mm^2)	6500-9200 (ballast size: 40~45 mm) 4400-6200 (ballast size: 30~35 mm)

	Surface texture	Surface texture index	1.35-4.12		Three dimensions (mm)	ballast size: 40~45 mm	Longest: 51-74 Intermediate: 43-61 Shortest: 32-55
						ballast size: 30~35 mm	Longest: 41-65 Intermediate: 35-48 Shortest: 29-44

The Surface texture index used in this paper is a modified method based on [32]. Because the method in [32] is only for the 2D particle images. It utilised the erosion–dilation technique, and the erosion–dilation technique has two steps. The first step is to remove pixels from the image based on the number of pixels surrounding it with different colours. The second step is to add pixels to the image. After the two procedures, the surface texture could not be restored, and then calculating the area difference can quantify the surface texture.

Using this principle, but with the 3D images, the Surface texture index (STI) is defined as the surface area difference after the 3D erosion-dilation technique, as shown in Figure 10. In Figure 10C, the red image is the particle image before the erosion-dilation technique, and the green is the image after the technique. The Surface texture index is quantified with the following equation.

Equation 3 $$STI = (A_1 - A_2) / A_1$$

In the equation, A_1 is the particle surface area before the erosion-dilation technique, while A_2 is the surface area after the technique.

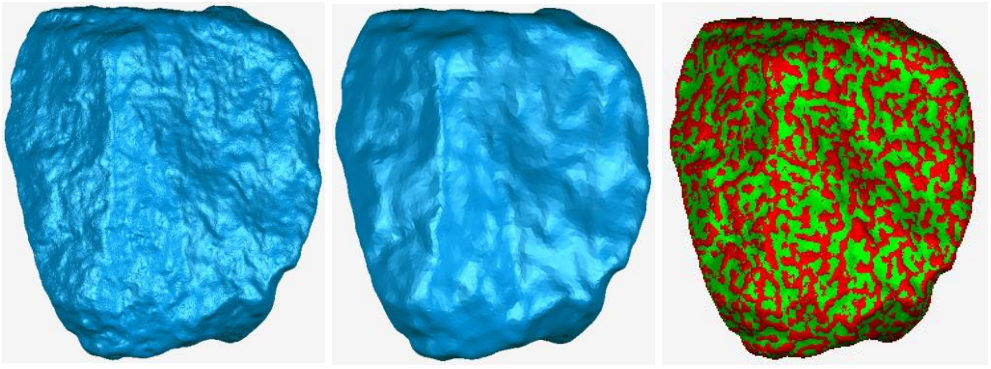

A. Before erosion-dilation technique B. After erosion-dilation technique C. Two images' comparison

Figure 10 The erosion-dilation technique for 3D image of ballast particle

Using the introduced morphological indices, the morphology can be quantified and the quantified values are given in Appendix A (Table A.5). Afterwards, the particles with similar values are selected for the degradation analysis, and the ranges of the values are given in Table 3. As introduced in Section 2.2.3 (Image analysis method), the abrasion is analysed with the Abrasion Depth, while the breakage analysis is performed with the new method.

3.2.3 Abrasion Depth

The Abrasion Depth results (MAD, AAD) of all the scanned ballast particles are given in Appendix A (Table A.3). Using this table and Table A.5, the abrasion values of the selected particles (with similar morphology) were picked out for analysis, shown in Table A.6. It needs to note that the non-cubic particles, large corner loss particles or the broken particles were not picked out. The large corner loss particles are not picked out, because it is difficult to identify that is caused by sharp corner breakage or abrasion.

According to the results in Table A.6, the correlation between AAD results and the CR size/percentage is shown in Figure 11. From the figure, it can be seen that the CR can reduce the ballast abrasion, in most cases. In addition, increasing CR percentage mostly leads to smaller AAD value. However, when the CR percentage is over 10%, the percentage effects on the AAD value are not significant (Figure 11 A/C). Interestingly, the CR size at the range of 20~25 mm has the least influence on the AAD values of ballast particle size at 30~35 mm (Figure 11 B/D). That means when the CR size is close to the ballast size, the CR has a slight influence on the ballast abrasion. Concerning the ballast material, the 3~5 mm CR is better to reduce the abrasion of volcanic ballast particles of than granite ones.

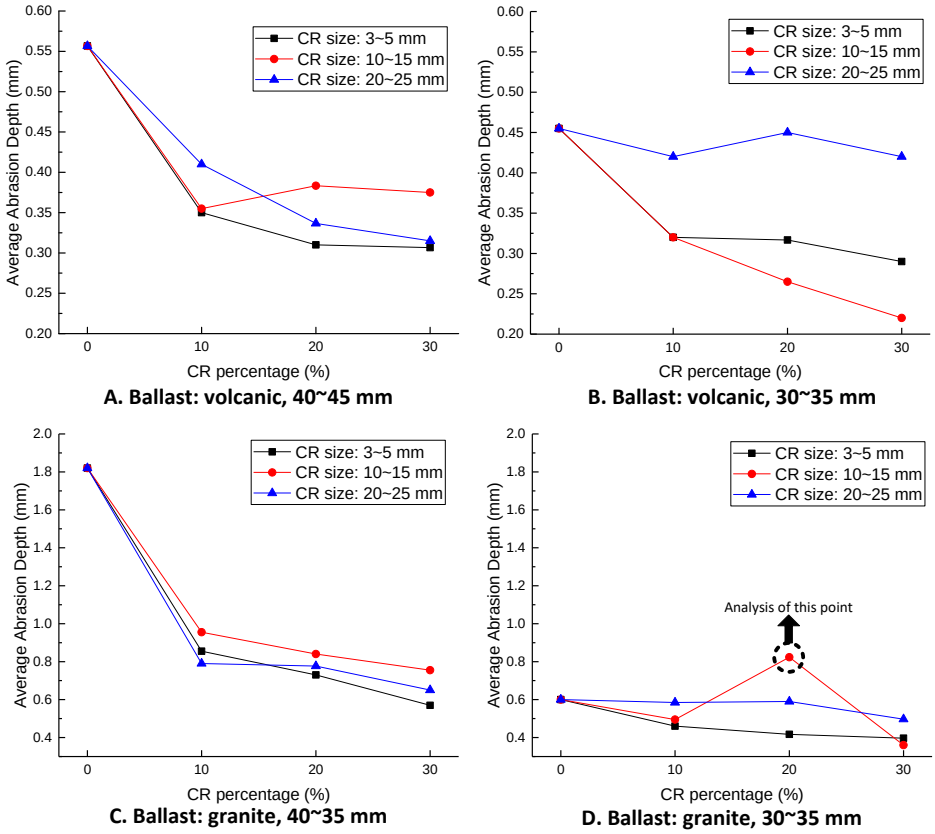

Figure 11 Correlation between Average Abrasion Depth results and CR size/percentage

In Figure 11D, the marked point is analysed, because its value is anomalous. The value is calculated with the average of the three particles' AADs in Group 38, and all the three AADs are high. Five particles in one group were scanned, but three particles were selected in Group 38 because the other two particles are non-cubic and broken, respectively.

After the three ballast particles were checked (Figure 12), Figure 12 A/B shows that the high abrasion part is not only the edge and corner but also the surface. That is due to a slice dropped during the test because of the initial micro-crack. Additionally, in Figure 12C, the edge and corner are sharper than particles in other groups, even though their Roundness values are similar. That means it is not sufficient for some particular particles to use the Roundness for angularity quantification. However, to date, no studies were found to quantify both the 3D angularity and the edge. Most importantly, it cannot be judged clearly that the corner loss was caused by the abrasion or breakage. Therefore, more studies should be performed on the particle morphology evaluation with 3D images. Also, more research should focus on how ballast degradation relates to the initial condition of the ballast particle, e.g. the initial micro-crack.

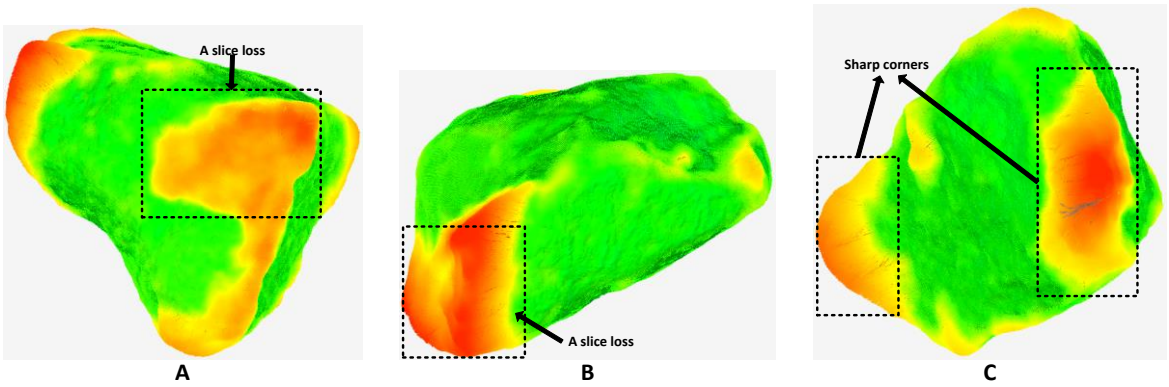

Figure 12 Ballast particle abrasion in the Group 38

Figure 13 shows the correlation between Maximum Abrasion Depth and CR size/percentage. From the figure, it can be seen that adding CR could reduce the angularity reduction in most cases (presented as lower MAD value) except the 20~25 mm CR. In Addition, the particle size at 40~45 mm has more MAD reduction than the 30~35 mm. The higher percentage of 3~5 mm CR can reduce the MAD value more, however, the optimal percentage of the other two CR cannot be determined. Because the sharpness of the corner was not fully quantified, and it has more effects on the particle abrasion than the CR percentage, especially for ballast material at the granite.

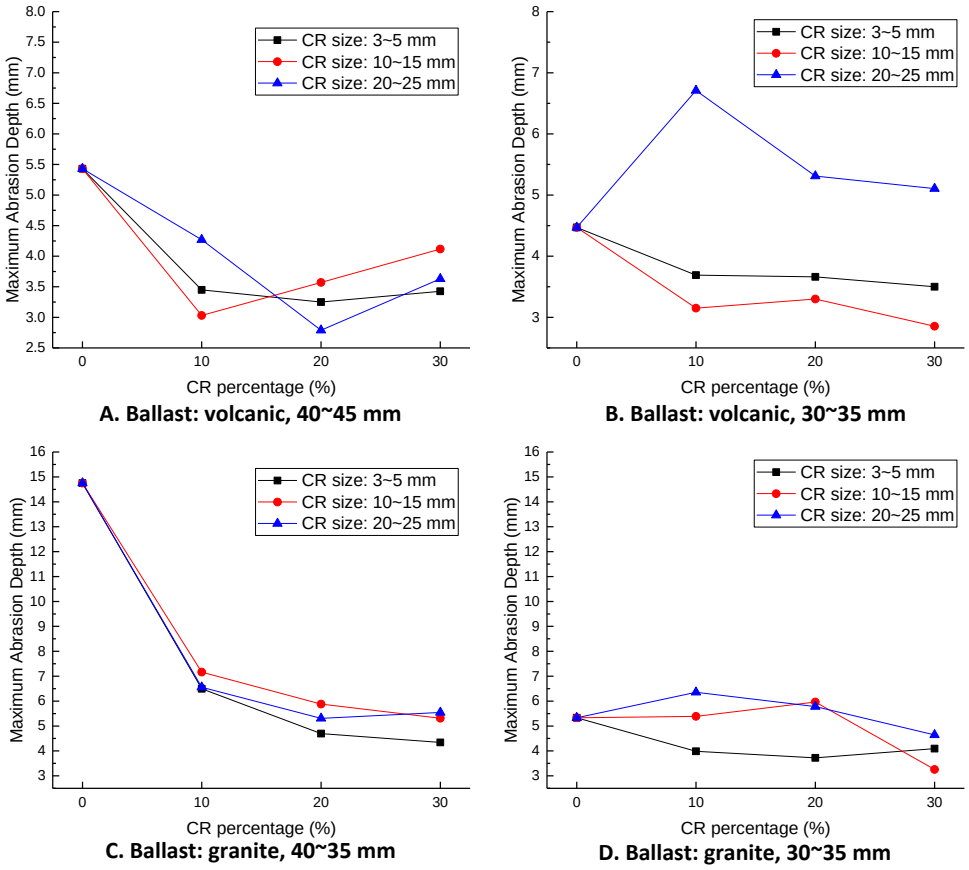

Figure 13 Correlation between Maximum Abrasion Depth and CR size/percentage

As shown in Figure 14, the different ballast degradation stages are illustrated. From the figure, it can be seen that after the first 1000 LAA drum turns, all the sharp corners are lost. Moreover, the first 1000 turns have severer abrasion than the second 1000 turns. Particularly, the part that suffers more abrasion is not definite during the second 1000 turns. That means at the early stage, the ballast

particles lose the sharp corner and edge. Afterwards, even though the corner and edge still dominate degradation, the surface texture becomes more significant, especially the bulge (large texture, Figure 14A).

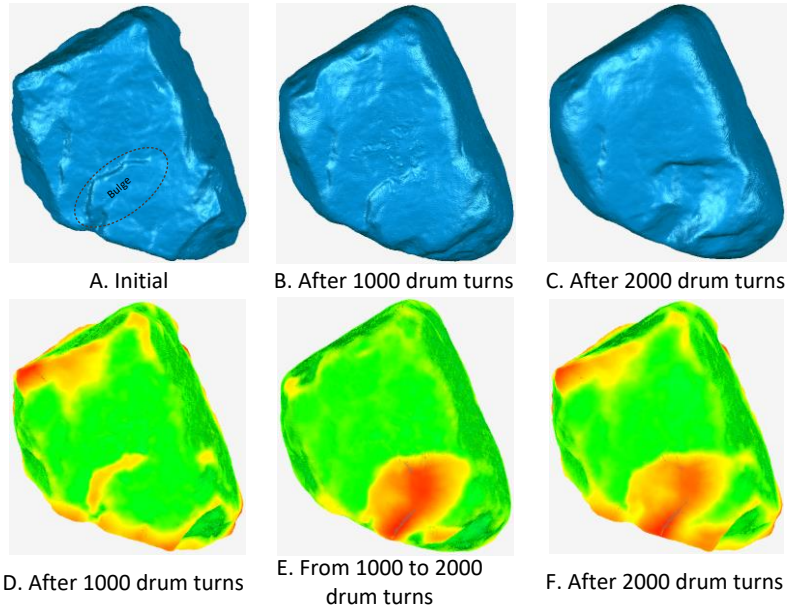

Figure 14 Ballast degradation at different LAA drum turns

3.2.4 Breakage analysis

The total volume and surface area of broken particles are given in Table A.7. According to the volume and the surface area, the Breakage Index (BI) is calculated with Equation 3. In this table, the initial images of the broken particles were checked to find out the relation between particle morphology and breakage. Additionally, the images of broken particles were analysed to confirm the breakage type.

From the table, it can be observed that after the particle breakage, the total surface area increases, even though 1000 drum turns LAA tests were performed on the broken particle. Also, the BI can present the breakage degree and type. For example, as shown in Figure 15, three types and their BI values are given including the breaking into pieces, at the middle and corner loss.

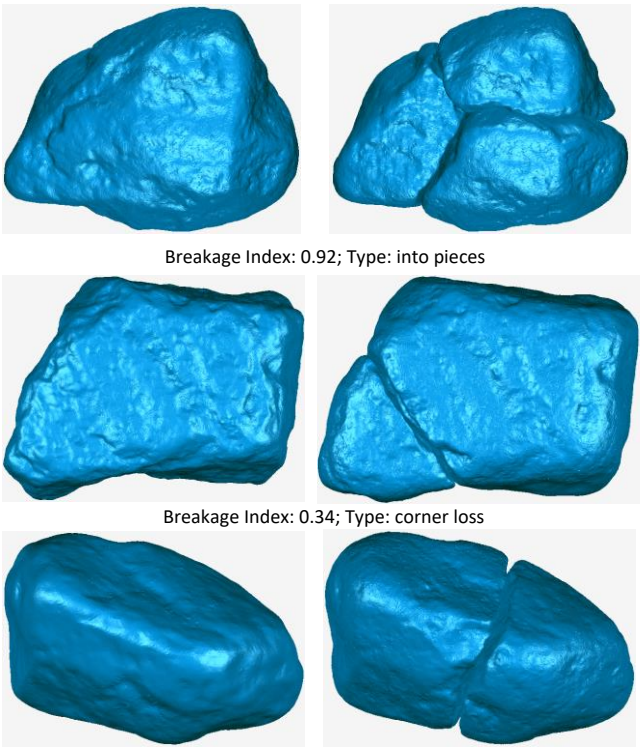

Figure 15 Three types of particle breakage and their values of the Breakage Index

After analysing the BI results, it is found that adding the CR has few influences on the ballast breakage. Also, the correlation between the CR size/percentage and the ballast breakage is difficult to verify. Because the ballast breakage is more related with initial micro-cracks and particle morphology. Additionally, the corner loss is difficult to distinguish as abrasion or breakage.

Regarding the correlation between morphology and breakage, the non-cubic ballast particles are more prone to crush and usually break at the middle or into pieces, e.g. No. 3/8/10/12/17/20 in Table A.7. The non-cubic particles have low 3D True Sphericity and Roundness values, however, when checking the 3D True Sphericity and Roundness of the broken particles, no strong correlations are found between the two indices and breakage.

Even though some particles are with higher values of the two indices, they were crushed because of the weak point or initial micro-cracks. The weak point is the part that is easy to break, e.g. the sharp corner (No. 4/32/37, Table A.7), while the initial micro-crack means the ballast particle has small initial micro-crack before the tests, which are difficult to observe. However, to date, the weak point cannot be evaluated accurately based on current image analysis methods. Additionally, the inner micro-crack is difficult to detect, and few studies were found in this direction.

The results are compared with those from literature [10, 11], and it is found that the experimental test type and test procedure have great influences on the results, especially for the ballast breakage alleviation. In [10, 11], it is proved that the ballast particle breakage decrease with the crumb rubber percentage increment. Whereas, the breakage alleviation is not obvious when increasing the CR percentage in this study. Besides the difference of the experimental tests (LAA test, ballast box test), other differences could also have great influence, such as the ballast material, ballast particle size and crumb rubber size. Therefore, further studies can be in these directions.

Conclusion and perspective

Conclusion:

The present research focuses on the analysis of ballast degradation of the CR and ballast mixtures with the aim of studying the optimal CR size and percentage. For this purpose, the LAA test was performed for impacting the mixtures, while the 3D image analysis method is utilised for degradation evaluation. Based on the results of this research, the following conclusions can be made:

- Ballast abrasion can be alleviated by adding the CR, while the CR has few influences on the ballast breakage. When the CR percentage is over 10%, it does not have significant effects on the ballast degradation reduction, especially for the larger size CR (approximates to ballast size).
- The first stage of ballast degradation is at the corner and edge, afterwards, the surface texture reduction becomes significant. With the CR, in the first stage (first 1000 turns), some of the easy loss parts can be protected, however, the long-term effects on degradation reduction (until 2000 turns) are not satisfactory.
- Ballast breakage type is more related to the initial micro-cracks and particle morphology, and morphology evaluation methods based on image analysis can identify the weak points of ballast particles.

Perspective:

- To perform other kinds of experimental tests on the CR-ballast mixture are considered as the next research step, such as the cyclic triaxial test, ballast box test and field test. The ballast degradation after these tests will be quantified and compared with the results in this paper.
- Morphological index for angularity and edge quantification with 3D images is requisite for the ballast degradation-related studies.
- Using X-ray computed tomography combined with 3D images could evaluate and predict the ballast degradation more convincingly because the X-ray computed tomography can detect the initial micro-cracks. Although in this paper, the particle morphology is considered, however, the initial micro-cracks before the tests were not tested or quantified. That also has significant influences on the results.
- Discrete element method (DEM) analysis is necessary for the ballast degradation study, because it can control variables. Some of the variables are difficult to control in tests, e.g. the angularity. The breakage type will be utilised into a DEM model to present degradation more reliably.

Acknowledgments

The paper is supported by the Chinese Scholarship Council and the Natural Science Foundation of China (Grant No.51578051). We would like to thank Zhejiang Tiantie Industry and Ruihai 3D technology limited company for their kind help to this research. We would also like to thank Luchao Qie from CARS for his help to paper modification.

Reference

[1] D. Li, J. Hyslip, T. Sussmann, S. Chrismer, Railway geotechnics, CRC Press2002.
[2] B. Indraratna, W. Salim, C. Rujikiatkamjorn, Advanced rail geotechnology: Ballasted track, CRC press London2011.
[3] Q.D. Sun, B. Indraratna, S. Nimbalkar, Deformation and Degradation Mechanisms of Railway Ballast under High Frequency Cyclic Loading, Journal of Geotechnical and Geoenvironmental Engineering 142(1) (2016) 04015056.
[4] M. Sol-Sánchez, F. Moreno-Navarro, M.C. Rubio-Gámez, Viability of using end-of-life tire pads as under sleeper pads in railway, Construction and Building Materials 64 (2014) 150-156.

[5] M. Sol-Sánchez, F. Moreno-Navarro, M.C. Rubio-Gámez, The use of elastic elements in railway tracks: A state of the art review, Construction and Building Materials 75 (2015) 293-305.
[6] M. Sol-Sánchez, G. D'Angelo, Review of the design and maintenance technologies used to decelerate the deterioration of ballasted railway tracks, Construction and Building Materials 157 (2017) 402-415.
[7] B. Indraratna, S.K.K. Hussaini, J.S. Vinod, The lateral displacement response of geogrid-reinforced ballast under cyclic loading, Geotextiles and Geomembranes 39 (2013) 20-29.
[8] R. Sañudo, L. dell'Olio, J.A. Casado, I.A. Carrascal, S. Diego, Track transitions in railways: A review, Construction and Building Materials 112 (2016) 140-157.
[9] G. Jing, L. Qie, V. Markine, W. Jia, Polyurethane reinforced ballasted track: Review, innovation and challenge, Construction and Building Materials 208 (2019) 734-748.
[10] M. Sol-Sánchez, N.H. Thom, F. Moreno-Navarro, M.C. Rubio-Gámez, G.D. Airey, A study into the use of crumb rubber in railway ballast, Construction and Building Materials 75 (2015) 19-24.
[11] M. Fathali, F.M. Nejad, M. Esmaeili, Influence of Tire-Derived Aggregates on the Properties of Railway Ballast Material, Journal of Materials in Civil Engineering 29(1) (2017) 04016177.
[12] C. Hidalgo Signes, P. Martínez Fernández, E. Medel Perallón, R. Insa Franco, Analysis of the vibration alleviation of a new railway sub-ballast layer with waste tyre rubber, Materials and Structures 50(2) (2016).
[13] S.D. Cho, J.M. Kim, J.H. Kim, K.W. Lee, Utilization of waste tires to reduce railroad vibration, Materials science forum, Trans Tech Publ, 2007, pp. 637-640.
[14] P. Martínez Fernández, C. Hidalgo Signes, I. Villalba Sanchís, D. Pérez Mira, R. Insa Franco, Real scale evaluation of vibration mitigation of sub-ballast layers with added tyre-derived aggregate, Construction and Building Materials 169 (2018) 335-346.
[15] M. Esmaeili, J.A. Zakeri, H. Ebrahimi, M. Khadem Sameni, Experimental study on dynamic properties of railway ballast mixed with tire derived aggregate by modal shaker test, Advances in Mechanical Engineering 8(5) (2016).
[16] C. Hidalgo Signes, P. Martínez Fernández, E. Medel Perallón, R. Insa Franco, Characterisation of an unbound granular mixture with waste tyre rubber for subballast layers, Materials and Structures 48(12) (2014) 3847-3861.
[17] J.L. Perez, C. Kwok, K. Senetakis, Effect of rubber size on the behaviour of sand-rubber mixtures: A numerical investigation, Computers and Geotechnics 80 (2016) 199-214.
[18] B.s.p.B.E. British Standards Institution, Aggregates for railway ballast, British Standards Institution London, 2013.
[19] T.P.M.o. Railways, Railway Ballast, TB/T2140-2008, China Railway Publishing House, Beijing, 2008.
[20] G. Jing, H. Fu, P. Aela, Lateral displacement of different types of steel sleepers on ballasted track, Construction and Building Materials 186 (2018) 1268-1275.
[21] X. Zhang, C. Zhao, W. Zhai, C. Shi, Y. Feng, Investigation of track settlement and ballast degradation in the high-speed railway using a full-scale laboratory test, Proceedings of the Institution of Mechanical Engineers, Part F: Journal of Rail and Rapid Transit (2018) 0954409718812231.
[22] C. Jayasuriya, B. Indraratna, T. Ngoc Ngo, Experimental Study to Examine the Role of Under Sleeper Pads for Improved Performance of Ballast under Cyclic Loading, Transportation Geotechnics (2019).
[23] Y. Qian, H. Boler, M. Moaveni, E. Tutumluer, Y.M. Hashash, J. Ghaboussi, Degradation-Related Changes in Ballast Gradation and Aggregate Particle Morphology, Journal of Geotechnical and Geoenvironmental Engineering 143(8) (2017) 04017032.
[24] R. Nålsund, Railway ballast characteristics, selection criterion and performance, Department of Civil and Transport Engineering, Norwegian University of Science and Technology, Trondheim (2014).
[25] B. Aursudkij, A laboratory study of railway ballast behaviour under traffic loading and tamping maintenance, University of Nottingham, 2007.
[26] G.R. McDowell, W.L. Lim, A.C. Collop, R. Armitage, N.H. Thom, Laboratory simulation of train loading and tamping on ballast, P I Civil Eng-Transp, Thomas Telford Ltd, 2005, pp. 89-95.

[27] W.L. Lim, Mechanics of railway ballast behaviour, University of Nottingham, 2004.
[28] J. Fernlund, 3-D image analysis size and shape method applied to the evaluation of the Los Angeles test, Engineering geology 77(1) (2005) 57-67.
[29] P. Tolppanen, 3-D Characterization and Degradation Analysis of Rock Aggregates, Institutionen för anläggning och miljö, 2001.
[30] Y. Guo, V. Markine, J. Song, G. Jing, Ballast degradation: Effect of particle size and shape using Los Angeles Abrasion test and image analysis, Construction and Building Materials 169 (2018) 414-424.
[31] Y. Guo, V. Markine, X. Zhang, W. Qiang, G. Jing, Image analysis for morphology, rheology and degradation study of railway ballast: A review, Transportation Geotechnics 18 (2019) 173-211.
[32] T. Al-Rousan, E. Masad, E. Tutumluer, T. Pan, Evaluation of image analysis techniques for quantifying aggregate shape characteristics, Construction and Building Materials 21(5) (2007) 978-990.
[33] D. Zhang, X. Huang, Y. Zhao, Investigation of the shape, size, angularity and surface texture properties of coarse aggregates, Construction and Building Materials 34 (2012) 330-336.
[34] J.K. Anochie-Boateng, J.J. Komba, G.M. Mvelase, Three-dimensional laser scanning technique to quantify aggregate and ballast shape properties, Construction and Building Materials 43 (2013) 389-398.
[35] T. Pan, E. Tutumluer, Imaging-based direct measurement of aggregate surface area and its application in asphalt mixture design, International Journal of Pavement Engineering 11(5) (2010) 415-428.
[36] C. Rao, E. Tutumluer, Determination of volume of aggregates: New image-analysis approach, Transportation Research Record: Journal of the Transportation Research Board (1721) (2000) 73-80.
[37] L. Wang, X. Wang, L. Mohammad, C. Abadie, Unified method to quantify aggregate shape angularity and texture using Fourier analysis, Journal of Materials in Civil Engineering 17(5) (2005) 498-504.
[38] Y. Guo, G. Jing, Ballast degradation analysis by Los Angeles Abrasion test and image analysis method, Bearing Capacity of Roads, Railways and Airfields: Proceedings of the 10 th International Conference (June 28–30, 2017, Athens, Greece), 1811.
[39] P. Barrett, The shape of rock particles, a critical review, Sedimentology 27(3) (1980) 291-303.
[40] Y. Hayakawa, T. Oguchi, Evaluation of gravel sphericity and roundness based on surface-area measurement with a laser scanner, Computers & Geosciences 31(6) (2005) 735-741.

Appendix A. Supplementary data

Table A.1 Basic characterisation of the ballast materials

Table A.2 Los Angeles Abrasion loss results

Table A.3 Image analysis results – volume, surface area and Abrasion Depth

Table A.4 Image analysis results – analysis of volume and surface area

Table A.5 Values of the morphological indices for morphology evaluation

Table A.6 Image analysis results for the selected particles

Table A.7 The images, volume and surface area of the broken ballast particles